Journal of Alloys and Compounds 498 (2010) 152–156

Contents lists available at ScienceDirect

Journal of Alloys and Compounds

journal homepage: www.elsevier.com/locate/jallcom

Enhancement of luminescence and afterglow in $CaTiO_3:Pr^{3+}$ by Zr substitution for Ti

Jun-Cheng Zhang, Xusheng Wang*, Xi Yao

Functional Materials Research Laboratory, Tongji University, 1239 Siping Road, Shanghai 200092, China

ARTICLE INFO

Article history:
Received 20 January 2010
Received in revised form 14 March 2010
Accepted 15 March 2010
Available online 23 March 2010

Keywords:
$CaTiO_3:Pr^{3+}$
Luminescence
Afterglow

ABSTRACT

The photoluminescence and afterglow characteristics of Zr doped $CaTiO_3:Pr^{3+}$ phosphors were investigated. Zr^{4+} substitution for Ti^{4+} leads to the enhancement of red fluorescence and phosphorescence at 613 nm originating from $^1D_2$ to $^3H_4$ transition of Pr^{3+}, and the increase of the lifetime for the $^1D_2$ state. The enhancement of emission intensity was attributed to the change of the lattice structure, the increase of the Pr^{3+} amount, and the decrease of the concentration of the defects quenching red emission. The increase of lifetime was thought to originate from the increase of the density of $[Pr_{Ca}]^0$ traps.

1. Introduction

To achieve new and excellent bright and long decay red-emitting phosphors is becoming more and more important for the various displays and signing application in the dark environments, since the green- and blue-emitting phosphors have been more developed than the red-emitting ones [1–5]. Recently, the red-emitting oxide phosphors with well chemical stability have been investigated extensively and developed rapidly to replace the traditional sulfide phosphors [6–9]. Among them, $CaTiO_3:Pr^{3+}$ is of special interest due to its red emission with appropriate CIE coordinate (0.680, 0.311), which is very close to that of the 'ideal red' [1]. To improve the luminescence intensity and enhance the afterglow efficiency of this perovskite material, many efforts have been done [2,3,10–15]. It is known that there exist two ways for increasing the emission intensity. The most effective way is making use of different charge compensators to balance Pr^{3+} ions. Using monovalent cations including Na^+, Tl^+, or Ag^+ substitution for Ca^{2+} [2], trivalent cations such as Al^{3+} [10] or Ln^{3+} (Ln = La, Lu, Gd) [11] substitution for Ti^{4+}, or using calcium vacancy compensation method [12] have been reported. Another way is to substitute Ca^{2+} with equivalent cations, such as Zn^{2+}, Mg^{2+} [3], Ba^{2+}, or Sr^{2+} [13]. On the other hand, the afterglow time of the red-emitting $CaTiO_3:Pr^{3+}$ phosphors can be enhanced by substituting Zn^{2+} for Ca^{2+} site [14,15], or Al^{3+} [16], Lu^{3+} [11] for Ti^{4+} site. The possible explanation is that the density of traps with reasonable depth increases in the host materials. However, it needs to refer that the effect of equivalent cation substitution for Ti^{4+} site on the luminescence property is seldom reported in $CaTiO_3:Pr^{3+}$ phosphors. Pinel et al. studied the reasons for the greenish-blue emission in $CaZrO_3:Pr^{3+}$ and red emission in $CaTiO_3:Pr^{3+}$ [17]. Yan and Zhou presented the Pr^{3+} concentration quenching phenomena in $CaTiO_3:Pr^{3+}$ and $CaTi_{0.5}Zr_{0.5}O_3:Pr^{3+}$ [18]. In this work, $CaTiO_3:Pr^{3+}$ with Zr^{4+} substitution for Ti^{4+} was synthesized by the conventional solid-state reaction method. It was observed that Zr^{4+} substitution could significantly enhance both the luminescence intensity and afterglow time at 613 nm. The Zr^{4+} addition effect on the enhancement of luminescence and afterglow was discussed.

2. Experimental

Powder samples with a stoichiometric composition of $Ca_{0.998}Pr_{0.002}(Zr_xTi_{1-x})O_3$ (where $x = 0$, 0.005, 0.01, 0.015, 0.02, 0.025, 0.05, or 0.07, hereafter denoted as $Ca(Zr_xTi_{1-x})O_3:Pr^{3+}$ for simplicity) were prepared by the conventional solid-state reaction method. Raw materials of $CaCO_3$, Pr_6O_{11}, TiO_2, and ZrO_2 (≥99.9%) were mixed thoroughly in the presence of ethanol. After drying, the mixture was prefired at 900 °C for 4 h in air, then crushed, and sintered at 1400 °C for 4 h in air.

The phase structure was identified by an X-ray diffractometer (XRD; D8 Advance, Bruker AXS GmbH). The photoluminescence (PL) spectra at room temperature were recorded using a spectrofluorometer (LS-55, PerkinElmer). The diffuse reflectance spectrum was measured using a UV/vis/NIR spectrophotometer (V-570, JASCO). Thermoluminescence (TL) curve was obtained on a thermoluminescence-meter (FJ427A1, Beijing Nuclear Instrument Factory). Heating rate for the curves is 2 K/s. The afterglow time was measured by a photon-counting system that consists of a photomultiplier tube (R649, Hamamatsu Photonics K.K.) and a photocounter (C3866, Hamamatusu Photonics K.K.) controlled by a computer. Before the measurements of TL curve and afterglow time, all the samples with the same weight were irradiated at 254 nm for 5 min with a 6-W conventional ultraviolet lamp. The 77 K emission spectrum and the decay time spectrum were taken on a spectrophotometer (FLS920, Edinburgh Instruments Ltd.). All measurements were performed at room temperature except TL and the 77 K emission spectra.

* Corresponding author. Tel.: +86 21 65980544; fax: +86 21 65985179.
E-mail address: xs-wang@tongji.edu.cn (X. Wang).

0925-8388/$ – see front matter © 2010 Elsevier B.V. All rights reserved.
doi:10.1016/j.jallcom.2010.03.138

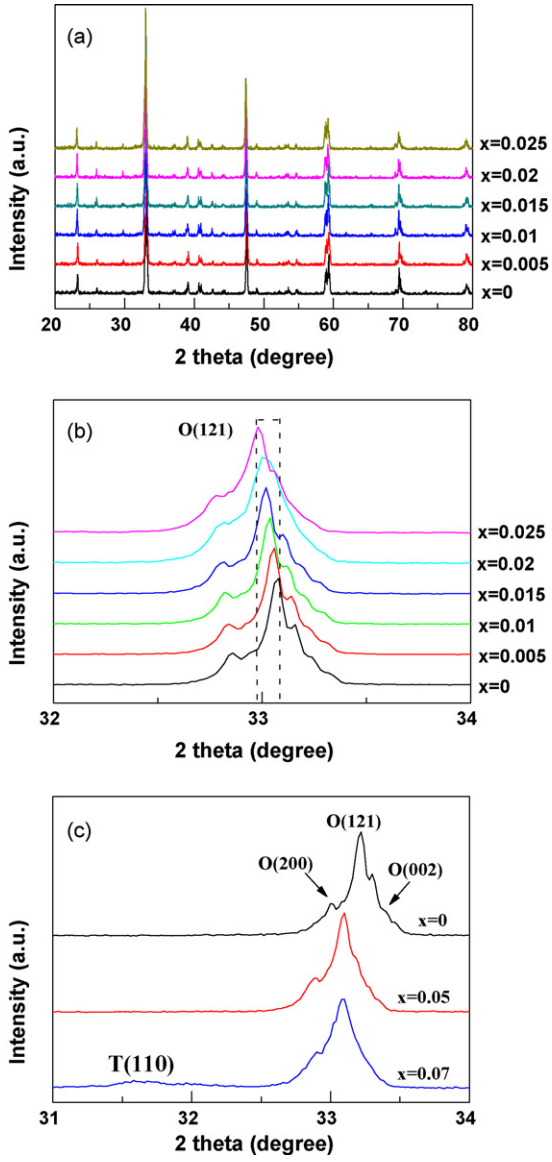

Fig. 1. XRD patterns of $Ca(Zr_xTi_{1-x})O_3:Pr^{3+}$ compositions (a) and refined peaks near orthorhombic peak (1 2 1) [labeled O(1 2 1)] (b) for $x = 0$, 0.005, 0.01, 0.015, 0.02, and 0.025. (c) Refined XRD patterns near the tetragonal peak (1 1 0) [labeled T(1 1 0)] and orthorhombic peak (1 2 1) for $x = 0$, 0.05, and 0.07.

3. Results and discussion

3.1. Phase characterization

The phase purity of the $Ca(Zr_xTi_{1-x})O_3:Pr^{3+}$ samples is shown in Fig. 1(a). The $CaTiO_3:Pr^{3+}$ phase is orthorhombic in structure (PDF #42-0423). There are no extra peaks observed in the XRD patterns of the Zr substitution samples, suggesting that Zr^{4+} ions have incorporated into the $CaTiO_3:Pr^{3+}$ lattice. Fig. 1(b) shows the scanned refinement XRD patterns near the strongest orthorhombic peak (1 2 1) [denoted as O(1 2 1)]. The O(1 2 1) peak shifts to the lower-angle side with increasing Zr content. It is attributed to the lattice expansion because of the larger size Zr^{4+} ion (CN6, 0.72 Å) substitution for Ti^{4+} (CN6, 0.605 Å). In Fig. 1(c), orthorhombic peaks of (2 0 0), (1 2 1), and (0 0 2) [denoted as O(2 0 0), O(1 2 1), and O(0 0 2), respectively] separate clearly for $CaTiO_3:Pr^{3+}$. However, the peaks of O(2 0 0) and O(0 0 2) gradually diminish with Zr addition, consistent with the change observed in Fig. 1(b). The peak intensities of O(2 0 0) and O(0 0 2) become negligible and the

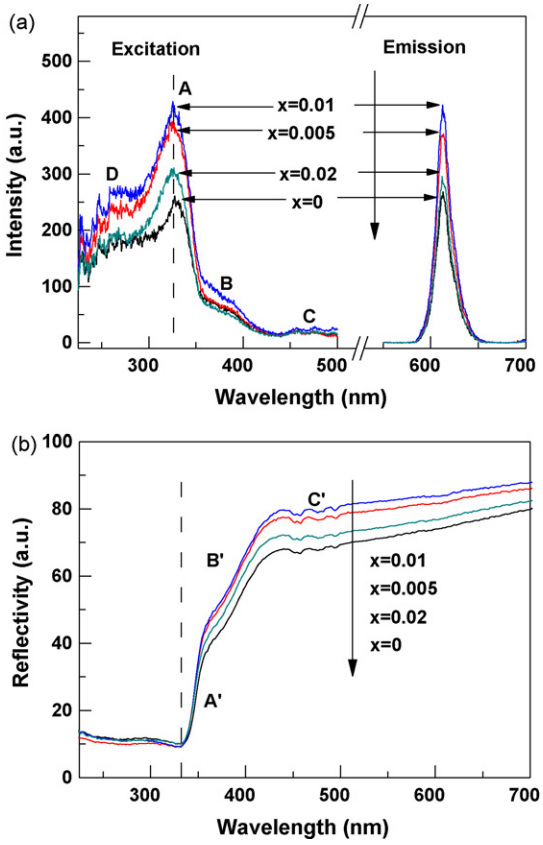

Fig. 2. (a) Excitation spectra (left) monitored at 613 nm and emission spectra (right) excited at 330 nm of $Ca(Zr_xTi_{1-x})O_3:Pr^{3+}$ samples at room temperature. (b) The diffuse reflectance spectra for the samples corresponding to $x = 0$, 0.005, 0.01, and 0.02 at room temperature.

tetragonal peak (1 1 0) [denoted as T(1 1 0)] appears when the Zr concentration reaches 7 mol%. These results indicate that Zr^{4+} substitution for Ti^{4+} has an effect on a lattice symmetry change from orthorhombic to pseudocubic.

3.2. Photoluminescence and optical properties

In order to investigate the influence of Zr addition on the luminescent properties, the excitation spectra, emission spectra, and the diffuse reflectance spectra at room temperature are depicted in Fig. 2. Fig. 2(a) shows the excitation spectra monitored at 613 nm (left) and the emission spectra excited by 330 nm light (right) for the $Ca(Zr_xTi_{1-x})O_3:Pr^{3+}$ phosphors. A sharp red emission at 613 nm can be observed for all the samples, due to the intra-4f transition from the excited $^1D_2$ to the ground state $^3H_4$ of Pr^{3+} [16]. The red emission of the phosphors depends strongly on the Zr concentration. The PL intensity enhances with increasing x value from 0 to 0.01. The PL integral intensity of the sample with $x = 0.01$ is the strongest, higher by 159% than that of $CaTiO_3:Pr^{3+}$. The red emission starts to decrease when x value exceeds this critical value, but it is still stronger than that of $CaTiO_3:Pr^{3+}$ until $x = 0.025$. Furthermore, in comparison with the positions of A′, B′ and C′ absorption bands in the diffuse reflectance spectra shown in Fig. 2(b), two strong broad bands centered at about 326 nm (A band) and 370 nm (B band), as well as the weak peaks (C band) at 456, 476, and 494 nm in the excitation spectra as labeled in Fig. 2(a) are consistent with them, respectively. The excitation band A is assigned to the valence-to-conduction band transition [O(2p)–Ti(3d)] according to the position of the absorption edge in the diffuse reflectance spectra [2]. It is worth to note that there is no change of the absorp-

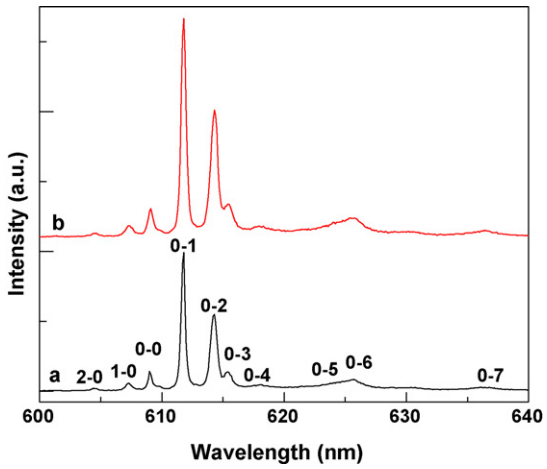

Fig. 3. Emission spectra of (a) $CaTiO_3:Pr^{3+}$ and (b) $Ca(Zr_{0.01}Ti_{0.99})O_3:Pr^{3+}$ [$^1D_2(0–2) \rightarrow {}^3H_4(0–7)$] excited at 330 nm at 77 K.

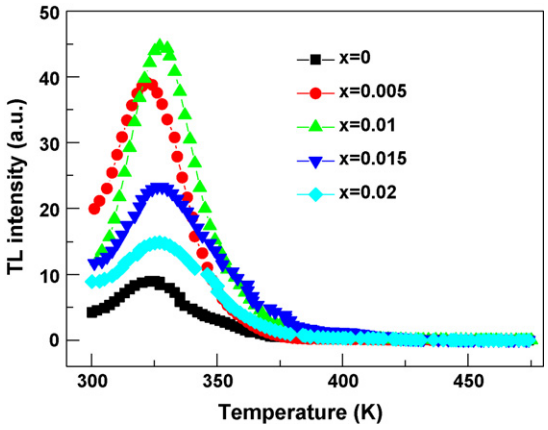

Fig. 4. Thermoluminescence glow curves of $Ca(Zr_xTi_{1-x})O_3:Pr^{3+}$ ($x = 0$, 0.005, 0.01, 0.015, and 0.02) after 5 min irradiation at 254 nm at room temperature.

tion edge by Zr^{4+} substitution for Ti^{4+}. This observation is different from the red shift of the absorption edge due to divalent metal ions, such as Ba^{2+} and Sr^{2+}, substitution for Ca^{2+} in $CaTiO_3:Pr^{3+}$ [13]. B band is attributed to a low-lying Pr-to-metal intervalence charge transfer state (IVCT), by which photo-electrons are radiationlessly de-excited from the $^3P_0$ state to the $^1D_2$ state of the Pr^{3+} ions [6,19]. The weak peaks (C band) at 456, 476, and 494 nm originate from $^3H_4$ to ^3P_J ($J = 0, 1, 2$) transitions, respectively [16]. Furthermore, the additional excitation band centered at 264 nm (D band) in Fig. 2(b) is ascribed to the lowest field component of the 4f5d state of Pr^{3+} [16,20,21].

There are two possible reasons for the enhancement of the PL intensity. One factor might be the change of the lattice symmetry. In the excitation spectra of Fig. 2(a), Zr substitution has a strong effect on enhancing the absorption of 4f5d levels of Pr^{3+} (D band) and valence-to-conduction band (A band) but little influence on the absorption of 4f–4f (C band). It indicates that the enhancement of red emission at 613 nm of Pr^{3+} is mainly due to the increase of the absorption of the 4f5d energy levels of Pr^{3+} and the conduction band of the host. Taking the change of the lattice symmetry induced by Zr^{4+} substitution for Ti^{4+} into consideration, the increase of the host absorption is associated with the lattice variation. Moreover, the change of the lattice symmetry will give rise to a remarkable effect on the local field around the Pr^{3+} and further influence the luminescence properties of Pr^{3+} [22,23]. It is well known that the 4f levels are well shielded by outer 5s- and 5p-electron shells and show a negligible interaction with the host, as shown in Fig. 3 which presents the emission spectra of $CaTiO_3:Pr^{3+}$ and $Ca(Zr_{0.01}Ti_{0.99})O_3:Pr^{3+}$ excited at 330 nm at 77 K. There is almost no difference in the $^1D_2(0–2) \rightarrow {}^3H_4(0–7)$ emission's peak locations and relative intensities between $CaTiO_3:Pr^{3+}$ and $Ca(Zr_{0.01}Ti_{0.99})O_3:Pr^{3+}$. However, the 4f5d band of Pr^{3+} is very sensitive to the host crystalline environment. The presence of a crystal field in most crystalline hosts would shift the 5d energy level of Pr^{3+} and allows more strong 4f–4f emission to occur [13,23]. The increased emission is shown in Fig. 3. The detailed mechanism should be investigated further. Another factor to improve the red emission is possibly owing to the increase of the Pr^{3+} amount and the decrease of the defects quenching red emission. It is known that Pr^{3+} can release an electron and be oxidized to Pr^{4+} while Ti^{4+} can get the electron and be reduced to Ti^{3+} when sintered in air, i.e. $Pr^{3+} - e \rightarrow Pr^{4+}$ and $Ti^{4+} + e \rightarrow Ti^{3+}$, or $Pr^{3+} + Ti^{4+} \rightarrow Pr^{4+} + Ti^{3+}$. A large amount of defects will form during the synthesis process. These defects are calcium vacancies ($[V_{Ca}]''$) to compensate $[Pr_{Ca}]^0$, Pr^{4+} ($[Pr_{Ca}]^{00}$) which tends to form by oxidization of Pr^{3+} after thermal treatment in air and negatively charged centers like Ti^{3+} ($[Ti_{Ti}]'$) and/or interstitial oxygen $[O_i]''$ correlated with the presence of Pr^{4+} [24]. Several defects are undesirable because they quench the Pr^{3+} luminescence dramatically even in low concentration. For example, part of the red emission can be reabsorbed by the broad $d \rightarrow d$ absorption band of Ti^{3+}. Furthermore, the positively charged defects can act as traps for electrons promoted in the conduction band after bandgap excitation. This electron capture constitutes an alternative radiationless de-excitation channel that competes with the energy transfer to the excited levels of Pr^{3+} and contributes to decrease the intensity of the $4f \rightarrow 4f$ emission. However, comparing with Ti^{4+}, Zr^{4+} is very stable and the valence state mixing 4+, 3+ is more difficult to occur in Zr ions. When Ti^{4+} is replaced by the stable Zr^{4+}, the number of Ti^{3+} oxidized from Ti^{4+} will decrease due to the reduce of the Ti^{4+} amount. On the other hand, according to the above-mentioned equations the number of Pr^{4+} will also decrease because of the decrease of the Ti^{3+} amount. Therefore, there are more Pr^{3+} and less undesired defects quenching the red emission, such as $[Pr_{Ca}]^{00}$, $[Ti_{Ti}]'$, and $[O_i]''$ which correlate with Ti^{3+} and Pr^{4+}. The red PL intensity is improved. This explanation is also supported by Fig. 2(a) and (b). In the diffuse reflectance spectra of $Ca(Zr_xTi_{1-x})O_3:Pr^{3+}$, it is clear that the absorption of the Zr substitution samples is less than that of $CaTiO_3:Pr^{3+}$ in the range of 420–700 nm, and the variation of the decrease of the absorption is consistent with the evolution of the enhancement of PL in the corresponding samples shown in Fig. 2(a), i.e. the sample with stronger PL intensity at 613 nm corresponding to the less absorption in the range of 420–700 nm.

3.3. Thermoluminescence and possible afterglow mechanism

TL curves of the $Ca(Zr_xTi_{1-x})O_3:Pr^{3+}$ phosphors in the temperature range of 300–475 K are shown in Fig. 4 to elucidate the effect of Zr^{4+} substitution on the afterglow. The profile and the location of the peak in the TL curve of $CaTiO_3:Pr^{3+}$ are consistent with previous reports [25,26]. With the increase of the Zr concentration, the profile of the curve and the location of the peak have not changed distinctly in comparison with those of $CaTiO_3:Pr^{3+}$, indicating that the type of traps responsible for TL has not changed. The one TL peak at around 325 K hints us that there is only a kind of traps contributing to the long phosphorescence existing in the investigated phosphors. Furthermore, the TL intensity is greatly affected by varying the Zr dopant concentration and it increases as the Zr dopant up to 1 mol%. The marked enhancement in TL shows that the concentration of the trapping center responsible for the TL glow peak increases due to Zr^{4+} substitution for Ti^{4+} in $CaTiO_3:Pr^{3+}$.

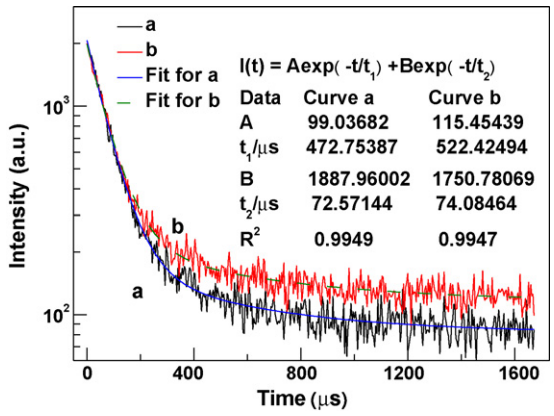

Fig. 5. Lifetime decay curves of the red emission (λ_{em} = 613 nm) in $CaTiO_3:Pr^{3+}$ (a) and $Ca(Zr_{0.01}Ti_{0.99})O_3:Pr^{3+}$ (b) at room temperature, excited at 330 nm.

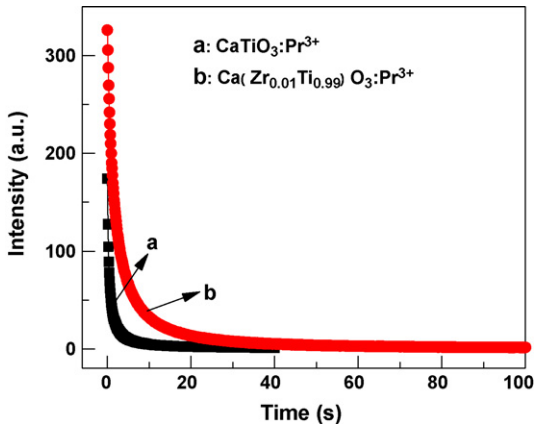

Fig. 6. Afterglow decay curves of $CaTiO_3:Pr^{3+}$ with Zr concentration of $x = 0$ (a) and $x = 0.01$ (b) after irradiation at 254 nm for 5 min at room temperature.

Afterglow is commonly supposed to correlate with trapping and thermal de-trapping of charge carriers at intrinsic or extrinsic defect centers [27]. For a given mobility of the charge carriers in the energy bands of the host, the storage capacity depends on the density of traps and on their trapping cross-section while the afterglow is determined by the density of population of these traps, the de-trapping rate and the capture cross-section of the recombination center. In the present case, the afterglow is mainly affected by the density of the traps around 325 K since there is no change in the traps' type and recombination center (Pr^{3+}). In $CaTiO_3:Pr^{3+}$, the trapping center responsible for the TL glow peak near the room temperature has been ascribed to be the positively charged $[Pr_{Ca}]^0$ defect [25]. This result was also confirmed by Boutinaud et al. [24]. They have pointed out that the $[Pr_{Ca}]^0$ defect plays a capital role in the afterglow process. The hole trapped by $[Pr_{Ca}]^0$ forms Pr^{3+}/h^+ ionic complex by reference to stable Pr^{4+} and the electron is trapped. Afterglow occurs after thermal de-trapping of the trapped electron and recombination with the Pr^{3+}/h^+ complex to form an excited Pr^{3+} ion that emits. In the case of Zr^{4+} substitution for Ti^{3+} in $CaTiO_3:Pr^{3+}$, the number of Pr^{4+} reduced from Pr^{3+} decreases due to Zr^{4+} substitution, so there are more Pr^{3+} ions in the Zr^{4+} substitution samples comparing with that in $CaTiO_3:Pr^{3+}$. Concomitantly, more Pr^{3+}/h^+ ionic complexes might be formed to increase the afterglow. Furthermore, about the TL concentration effect that the TL intensity decreases when the Zr concentration exceeds the optimal concentration (1 mol%), it is ascribed to the relationship between retrapping probability and concentration of electron traps. The retrapping probability may be negligible in the region of lower concentration but becomes predominant in the region of higher concentration.

Fig. 5 shows the lifetime decay curves of the red emission at 613 nm in Zr free sample (curve a) and 1 mol% Zr substitution for Ti sample (curve b) excited at 330 nm. The decay of the emission $^3H_4$ to $^1D_2$ at 613 nm consists of two different decay rates: the fast (fluorescent) and slow (phosphorescent) components. The decay curves can be well fitted by double exponential equation: $I(t) = A\exp(-t/\tau_1) + B\exp(-t/\tau_2)$, where I is the luminescence intensity, A and B are constants, t is the time, τ_1 and τ_2 are the fluorescent and phosphorescent decay time for the exponential components, respectively. The fitting results are also shown in Fig. 5. Furthermore, as shown in Fig. 6, the afterglow of $CaTiO_3:Pr^{3+}$ with 1 mol% Zr addition can be seen over 100 s by naked eyes, while the Zr free sample can only have a persistent time of 30 s for the red afterglow after the irradiation with a 6 W conventional ultraviolet lamp at 254 nm for 5 min. The above results clearly exhibit the increase of the phosphorescence lifetime by Zr substitution for Ti. They are consistent with the results of TL curves, supporting the proposal that more traps responsible for the afterglow exist in the case of the Zr substitution samples.

4. Conclusion

$Ca(Zr_xTi_{1-x})O_3:Pr^{3+}$ phosphors with Zr^{4+} substitution for Ti^{4+} were synthesized by the conventional solid-state reaction method. Their microstructure, optical, and afterglow properties were explored. The results indicate that Zr^{4+} addition induces a lattice symmetry change from orthorhombic to pseudocubic and can significantly enhance the red fluorescence intensity and the afterglow at 613 nm originating from $^1D_2$ to $^3H_4$ transition of Pr^{3+}. Both of the red fluorescence intensity and afterglow time reach the largest values in the sample with $x = 0.01$. The improvement of the PL intensity was ascribed to the change of the lattice structure, the increase of the Pr^{3+} amount, and the decreased concentration of the defects quenching red emission. The enhancement of the afterglow was explained by the increase of $[Pr_{Ca}]^0$ trapping centers because the number of Pr^{4+} reduced from Pr^{3+} decreased when unstable Ti^{4+} was replaced by stable Zr^{4+}.

Acknowledgements

This work was supported by the Natural Science Foundation of China (Nos. 50672067, 50932007), Scientific and Technical Innovation Program of Shanghai (No. 08JC1419100) and Specialized Research Fund for the Doctoral Program of Higher Education (No. 20070247010).

References

[1] S.S. Chadha, D.W. Smith, A. Vecht, C.S. Gibbons, 94 SID Digest 51 (1994) 1.
[2] P.T. Diallo, P. Boutinaud, R. Mahiou, J.C. Cousseins, Phys. Status Solidi A 160 (1997) 255.
[3] M.R. Royce, S. Matsuda, United States Patent (1997) 5,656,094.
[4] M. Wang, D. Wang, G. Lu, Mater. Sci. Eng. 18 (1998) B57.
[5] X.J. Wang, D.D. Jia, W.M. Yen, J. Lumin. 34 (2003) 102.
[6] P. Boutinaud, E. Pinel, M. Dubois, A.P. Vink, R. Mahiou, J. Lumin. 111 (2005) 69.
[7] S. Okamoto, H. Kobayashi, H. Yamamoto, J. Appl. Phys. 86 (1999) 5594.
[8] M. Iwasaki, D.N. Kim, K. Tanaka, T. Murata, K. Morinaga, Adv. Mater. 4 (2003) 137.
[9] J. Fu, Solid State Lett. 3 (2000) 350.
[10] J. Tang, X. Yu, L. Yang, C. Zhou, X. Peng, Mater. Lett. 60 (2006) 326.
[11] X. Zhang, J. Zhang, X. Zhang, L. Chen, S. Lu, X.J. Wang, J. Lumin. 122–123 (2007) 958.
[12] T. Li, M. Shen, L. Fang, F. Zheng, X. Wu, J. Alloys Compd. 474 (2009) 330.
[13] X. Wang, C.N. Xu, H. Yamada, Jpn. J. Appl. Phys. 44 (2005) L912.
[14] J. Zhi, A. Chen, L.K. Ju, Opt. Mater. 31 (2009) 1667.
[15] X. Yuan, X. Shi, M. Shen, W. Wang, L. Fang, F. Zheng, X. Wu, J. Alloys Compd. 485 (2009) 831.

[16] W. Jia, D. Jia, T. Rodriguez, D.R. Evans, R.S. Meltzer, W.M. Yen, J. Lumin. 119–120 (2006) 13.
[17] E. Pinel, P. Bountinaud, R. Mahiou, J. Alloys Compd. 380 (2004) 225.
[18] B. Yan, K. Zhou, J. Alloys Compd. 398 (2005) 165.
[19] P. Boutinaud, R. Mahiou, E. Cavalli, M. Bettinelli, J. Appl. Phys. 96 (2004) 4923.
[20] W.Y. Jia, A. Perez-Andujar, I. Rivera, J. Electrochem. Soc. 150 (2003) H161.
[21] X. Zhang, J. Zhang, M. Wang, X. Zhang, H. Zhao, X.J. Wang, J. Lumin. 128 (2008) 818.
[22] W. Jia, W. Xu, I. Rivera, A. Perez, F. Fernandez, Solid State Commun. 126 (2003) 153.
[23] S.Y. Kang, Y.H. Kim, J. Moon, K.S. Suh, D.J. Lee, S.G. Kang, Jpn. J. Appl. Phys. 48 (2009) 052301.
[24] P. Boutinaud, E. Pinel, R. Mahiou, Opt. Mater. 30 (2008) 1033.
[25] Y. Pan, Q. Su, H. Xu, T. Chen, W. Ge, C. Yang, M. Wua, J. Solid State Chem. 174 (2003) 69.
[26] P. Boutinaud, L. Sarakha, E. Cavalli, M. Bettinelli, P. Dorenbos, R. Mahiou, J. Phys. D: Appl. Phys. 42 (2009) 045106.
[27] S.W.S. Mc Keever, Thermoluminescence of Solids, Cambridge University Press, Cambridge, 1985.